Optics & Laser Technology 177 (2024) 111085

Contents lists available at ScienceDirect

Optics and Laser Technology

journal homepage: www.elsevier.com/locate/optlastec

Multi-parameter terahertz metamaterial sensors based on single-layer quarter ring patterns

Sijia Du [a,b,1], Xiaoman Li [b,c,d,1], Mohsin Raza [b,c,d], Chenlu Mao [b,c,d], Fulong Yao [b,c,d], Yinghao Yuan [a,*], Weiping Wu [b,c,d,**]

[a] Terahertz Technology Innovation Research Institute, Terahertz Spectrum and Imaging Technology Cooperative Innovation Center, University of Shanghai for Science and Technology, Shanghai 200093, China
[b] Laboratory of Thin Film Optics, Shanghai Institute of Optics and Fine Mechanics, Chinese Academy of Sciences, 390 Qinghe Road, Jiading District, Shanghai 201800, China
[c] State Key Laboratory of High Field Laser Physics, Shanghai Institute of Optics and Fine Mechanics, Chinese Academy of Sciences, 390 Qinghe Road, Jiading District, Shanghai 201800, China
[d] University of Chinese Academy of Sciences, Beijing 100049, China

ARTICLE INFO

Keywords:
Terahertz
Metamaterials
Multifunctionality
Sensors
Quality factor

ABSTRACT

A terahertz metamaterial sensor based on a single-layer quarter ring pattern is proposed to realize the simultaneous measurement of temperature, refractive index, and other parameters through a metasurface consisting of a patterned quarter ring gold layer and a silicon substrate. Field finite element numerical simulations were performed to analyse the transmission and reflection spectra. A two-parameter sensor combined with electric field distribution was realized using multiple peaks, thus revealing the physical mechanisms of the interaction in metamaterial structures. In addition, the effect of each geometrical parameter on the sensor performance is also simultaneously analysed to verify the optimal selection of structural parameters. On this basis, the sensors are theoretically analysed at different incidence and polarization angles, and the results show that the transmittance is not sensitive to the polarization angle. The simulation results show that the transmittance at the resonant frequencies of 0.48 THz, 0.64 THz, 0.79 THz and 1.04 THz are 93.7 %, 79.1 %, 38.4 % and 50.8 %, respectively, and the refractive index sensitivities at the resonant frequencies are 6.84 GHz/RIU, 7.42 GHz/RIU, 8.22 GHz/RIU and 32.11 GHz/RIU, and quality factor Q of 6.76, 9.63, 15.51 and 26.28, respectively. The devices proposed in this study are simple in structure, easy to fabricate, easy to miniaturize and can be integrated for sensitivity, multi-parameter sensors. They can be functionally designed for chemical and biological sensing and other important applications.

1. Introduction

Nowadays, infrared and microwave devices operating in both sides of the terahertz band have important applications in many fields such as communication [1,2], imaging [3] and detection [4]. However, the terahertz band lacks sufficient radiation sources and detection tools, and many questions remain to be explored [5]. In electronics, terahertz is known as millimeter and sub-millimeter waves, and in optics, it is known as far-infrared waves. Terahertz waves have many unique properties, which contain a variety of spectral information about the vibration and rotation of living matter such as proteins, DNA and so on [2]. Many materials have strong absorption and scattering properties in this band, leading to many terahertz imaging applications [6]. Terahertz imaging can not only reveal the shape but also the composition of the object. At the same time, compared with the kilo electron volt (keV) photon energy of X-rays, the photon energy of terahertz radiation is only Millielectron Volt (meV), which is much smaller than the energy of chemical bonding. Terahertz has the advantages of non-destructive and non-ionization, so it has an important research value for biological entities such as cells and tissues [7].

* Corresponding author.
** Corresponding author at: Laboratory of Thin Film Optics, Shanghai Institute of Optics and Fine Mechanics, Chinese Academy of Sciences, Shanghai 201800, China.
E-mail addresses: yhyuan@usst.edu.cn (Y. Yuan), wuwp@siom.ac.cn (W. Wu).
[1] These authors contributed equally to this work and should be considered co-first authors.

https://doi.org/10.1016/j.optlastec.2024.111085
Received 31 December 2023; Received in revised form 10 April 2024; Accepted 26 April 2024
Available online 9 May 2024

Due to the lack of natural materials in nature that can directly interact with terahertz waves, and the small response cross-sectional area of biological macromolecules in the terahertz band, the interaction with electromagnetic waves is very weak, resulting in insignificant spectral changes, which makes the detection very difficult [8,9]. At the beginning of the 21st century, a British physicist John B. Pendry first proposed electromagnetic metamaterials with negative refractive indices and introduced the phenomenon of negative refraction as well as the concept of perfect lensing [10]. This led to many important and new concepts and applications, such as artificial terahertz electromagnetic materials [5], terahertz metamaterials [11], terahertz biosensors [12] and terahertz perfect absorbers [13]. They can be used for inducing electromagnetic waves through metallic windings, conductors, and open-loop resonators (SRRs) [13,14] to induce electromagnetic waves exhibiting perfect lensing, negative refraction, perfect absorption [12,15], electromagnetically induced transparency, and other electromagnetic properties, showing unprecedented flexibility in modulating light [16] and electromagnetic waves [17].

According to different application requirements, researchers managed to achieve highly sensitive detection and modulation of terahertz waves by modulating metasurface structures and materials [18,19]. For many years, biosensors have been a focus of research because of their cost-effectiveness, ease of use, small size and fast response characteristics [12]. Among the existing biosensors, metasurface based terahertz detection methods have been widely used in the field of biosensing, thus improving the sensitivity of terahertz biosensing detection [20–22]. In one of previous studies, rapid and highly sensitive detection of biomedical samples was achieved by local magnetic field enhancement with artificial electromagnetic structures [20].

Refractive index is an important physical parameter reflecting the type, concentration, biochemical reaction and optical properties of a substance. Refractive index sensor has a wide range of applications in fields such as environmental monitoring, biomedicine and food control. The refractive index varies with temperature, and accurate measurement of the refractive index needs to be carried out at constant temperature, which is not feasible in practice [23]. To achieve simultaneous detection of temperature and refractive index, it is necessary to have explicit requirements for multiple peaks in the spectrum, at least two or more peaks that are highly stable to temperature and refractive index changes. The localized surface plasmon resonance (LSPR)-based optical sensing technology has the advantages of portability, labeling-free, high sensitivity, fast response, and low cost, which enables highly sensitive detection of biomolecule actions on a tiny scale [24]. Several studies on the simultaneous detection of refractive index and temperature have been carried out by rationally designing the geometry and layout of the metamaterial cell, the local electromagnetic resonance response can be improved, resulting in a subwavelength resolution more favorable for temperature and refractive index detection and a significant increase in the sensitivity of the sensor [11].

In this paper, we present a multiparametric terahertz metamaterial sensor that allows simultaneous detection of temperature, refractive index, and other parameters on existing terahertz metasurfaces [25]. By graphical design, displacement currents dissimilar to those of metals can be introduced into the device, resulting in sharp resonance peaks and high-quality factor resonance. Free electrons in metal are excited by the incident light, electromagnetic waves coupled to free electrons on a metal surface form a near-field electromagnetic wave that propagates along the metal surface, and they are called surface plasmon resonance (SPR) [26]. To produce the LSPR effect, the particle size has to be smaller than the incident wavelength. And if this electromagnetic field is confined to a very small area of the metal surface, it is LSPR, and in order to produce the LSPR effect, the particle diameter must be smaller than the incident wavelength. In this case, metals are ideal for the preparation of LSPR because of their favorable physicochemical properties [27,28]. In addition, the shape of the metal structure determines the direction of the surface current. Selective absorption and scattering of light can be achieved, forming resonance peaks. The advantages of this sensor are simple structure, low fabrication cost, high quality factor, clear peaks and high sensitivity.

2. Architecture and theory

By detecting small changes in the dielectric properties of the surface of the metamaterial (manifested as frequency shifts in the transmission peaks of the terahertz wave propagation spectrum), information such as the temperature and refractive index of the surrounding environment can be obtained. In practical detection, in addition to factors such as the material type and concentrations of the ambient medium, the temperature is also affected. Therefore, a two-parameter measurement using multiple resonance peaks is performed to obtain the relationship between refractive index sensitivity and temperature sensitivity [29]. The corresponding refractive index changes can be obtained by measuring the two parameters, the process can be described as [23],

$$\frac{d\lambda_i}{dn}\times\Delta n+\frac{d\lambda_i}{dn}\times\frac{dn}{dT}\times\Delta T+\frac{d\lambda_i}{dT}\times\Delta T=\Delta\lambda_i(i=1,2) \tag{1}$$

where n is the ambient medium's refractive index, T is the temperature, and i ($i = 1,2$) are the two resonance peaks. The first is the independent variation of RI in the environment, the second is the thermal optical effect of the environment, and the third is the independent temperature variation. The equation can be further expressed as follows [30],

$$\begin{bmatrix}\Delta n+\dfrac{dn}{dT}\times\Delta T\\ \Delta T\end{bmatrix}=\begin{bmatrix}K_{n,1} & K_{T,1}\\ K_{n,2} & K_{T,2}\end{bmatrix}^{-1}\begin{bmatrix}\Delta\lambda_1\\ \Delta\lambda_2\end{bmatrix} \tag{2}$$

The performance of the sensor depends on its sensitivity and quality factors. The sensor sensitivity is defined by the change in frequency per refractive index unit (RIU) and is calculated as follows,

$$S=\frac{\Delta f}{\Delta n} \tag{3}$$

where Δf is the offset of the resonance peak and Δn is the refractive index.

The figure of merit (FOM) is an important parameter of the sensing performances [29], the expression to caculate FOM is given below,

$$FOM=\frac{S(f)}{FWHM} \tag{4}$$

where FWHM is the full width at half maximum.

The quality factor (Q-factor) of the terahertz metamaterial sensor can be calculated by the following equation,

$$Q=\frac{f}{FWHM} \tag{5}$$

Currently, metal-based metamaterials usually have low Q, due to the high loss and Joule heating effect of the plasmonic materials, which limit their applications for sensors. By designing special symmetrically arranged metal patterns, it is possible to enhance their near-field coupling effect, strengthen local resonance, and improve the sensitivity of sensors. Free-electron-rich silicon is chosen as the bottom substrate, whose internal carrier distribution can be flexibly adjusted in response to various external stimuli, thus conveniently influencing the transmission characteristics of the incident terahertz wave [31,32]. The vast majority of reported terahertz metal arrays are grown on silicon substrates, which have low loss and high quality factor when resonating with resonance drift-prone metals [17,33]. Since there are a large number of active electrons inside the metal, the free electron gas model is used to describe the law of motion of the active electrons inside the metal and its equation of motion is expressed as follows [34],

$$m\frac{dx^2}{d^2t}+m\gamma\frac{dx}{dt}=eE_0\exp(-iwt) \tag{6}$$

where m represents the mass of the electron, e is the amount of charge and γ is the damping coefficient. Using the Eq. (6), the expression for x can be solved,

$$x=-\frac{e}{mlw^2+irw}E \tag{7}$$

The relation between $x=\frac{n\cdot e\cdot x}{\varepsilon_0 E}$ and $w_p^2=\frac{ne^2}{m\varepsilon_0}$ in Eq. (7), did not consider the influence of the transition to the dielectric constant of the band, so the relative dielectric constant can be caculated by Eq. (7),

$$\varepsilon=1-\frac{w_p^2}{w^2+irw} \tag{8}$$

where w_p is the volume plasma frequency and γ is the metal loss factor representing the absorption loss.

As mentioned above, several resonance peaks are necessary to detect both changes in refractive index and temperature changes. Therefore, we have numerically simulated and analysed the design of metamaterial using the field finite element method (FEM). In the simulation, the incident electric field is assumed to be x-polarized, the boundary conditions are periodic in the x and y directions of the source incidence, ports are set up in the z direction as the source of incidence and the source of detection, an adaptive fine mesh is employed, and the effects of scattering are mitigated using scattering boundary conditions and perfectly matched layers. As shown in Fig. 1, the schematic of Fig. 1a and b shows the structure of a metasurface with the shape of a single-layer quarter ring, where the incident light propagates along the z-direction. On the top is a 'single-layer quarter ring' pattern using 0.2 μm thick gold material, and the top gold layer is considered as a Drude-type dispersion [35], substituting into Eq. (8), where the high-frequency permittivity, plasma frequency, and collision frequency are $\varepsilon_\infty = 1.0$, $w_p = 1.36\times10^{16}$ rad/s and $\gamma = 3.33\times10^{13}$ rad/s, respectively [12]. the bottom is a 250-μm thick low-loss silicon substrate.

3. Results and discussion

Fig. 2 shows the simulated transmittance and absorption spectra. From Fig. 2a and 2b, we observe four resonance peaks at 0.48, 0.64, 0.79, and 1.04 THz, and the transmittances of the structure are about 93.7 %, 79.1 %, 38.4 %, and 50.8 %, respectively, based on the TE polarized wave. From the absorption spectrum, a higher resonance enhancement is seen to be produced at 1.04 THz, and the variation of this point will be observed subsequently.

To study the origin of the peaks in more detail, we investigated the electron field distributions at the resonance frequencies to understand the sensing mechanism. Fig. 3 shows the cross-sectional distribution of the electric field in the cell. The electron field is distributed along the edges and longer parts of the single-layer quarter ring-shaped structure, indicating that the electron field resonance is concentrated in certain parts of the metal structures [12,15]. From the distribution of the electron field in Fig. 3a-3d, it can be seen that the direction of the electric field at 0.48, 0.64 and 0.79 THz is right-to-left, whereas the direction of the electric field at 1.04 THz is left-to-right. The localized electric fields at 0.48 and 0.64 THz are mainly concentrated in the gaps of the patterns. Similar to the distribution of the electric field, the charge density on the surface of the pattern is confined to the slits. Due to the high symmetry of the proposed structure, the incident electric field excites the electric quadrupole resonance. As the wavelength decreases

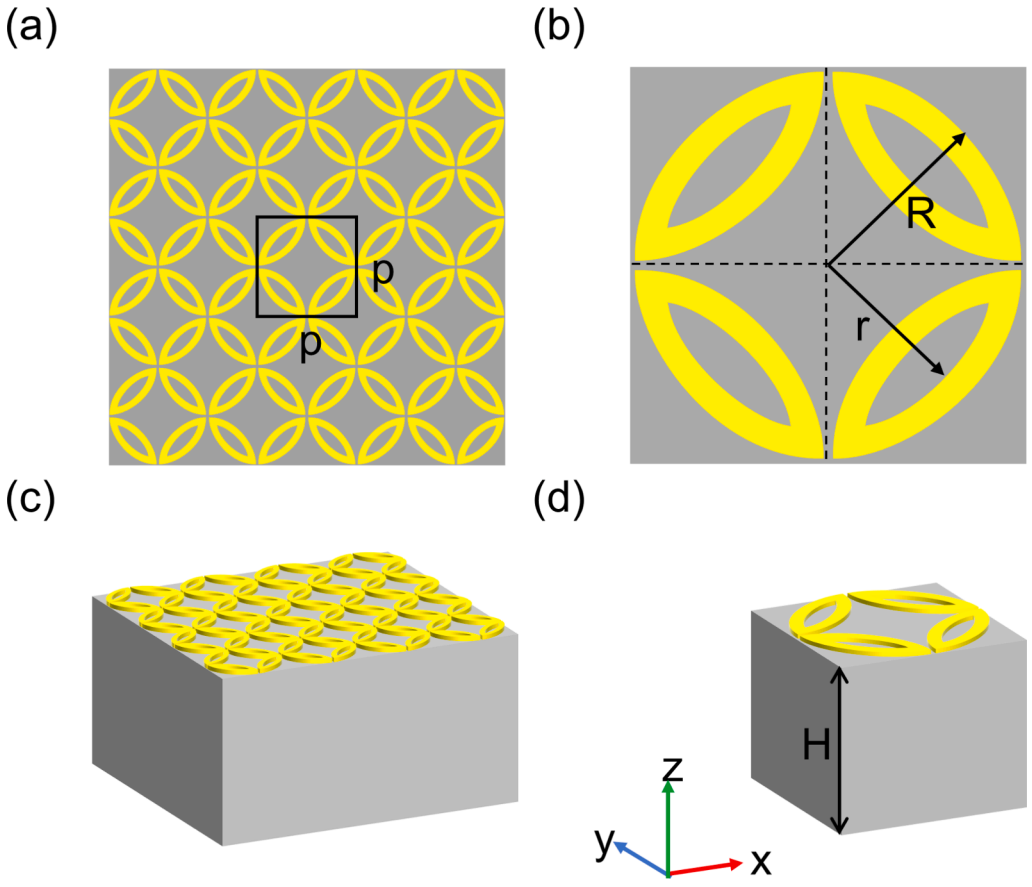

Fig. 1. Top view of (a) the metamaterial periodic structure, (b) the unit cell structure. 3D view of (c) the metamaterial periodic structure and (d) the unitary structure. The thickness of gold for the 'quarter ring' is 200 nm, the period p = 110 μm, and the radii of circles forming 'quarter ring' R = 58 μm and r = 50 μm.

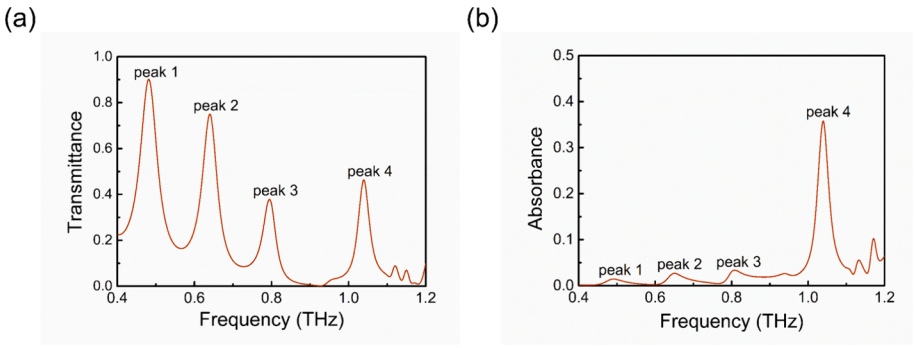

Fig. 2. (a) Simulated transmittance spectrum for TE-polarized waves, (b) Simulated absorbance spectrum for TE-polarized waves.

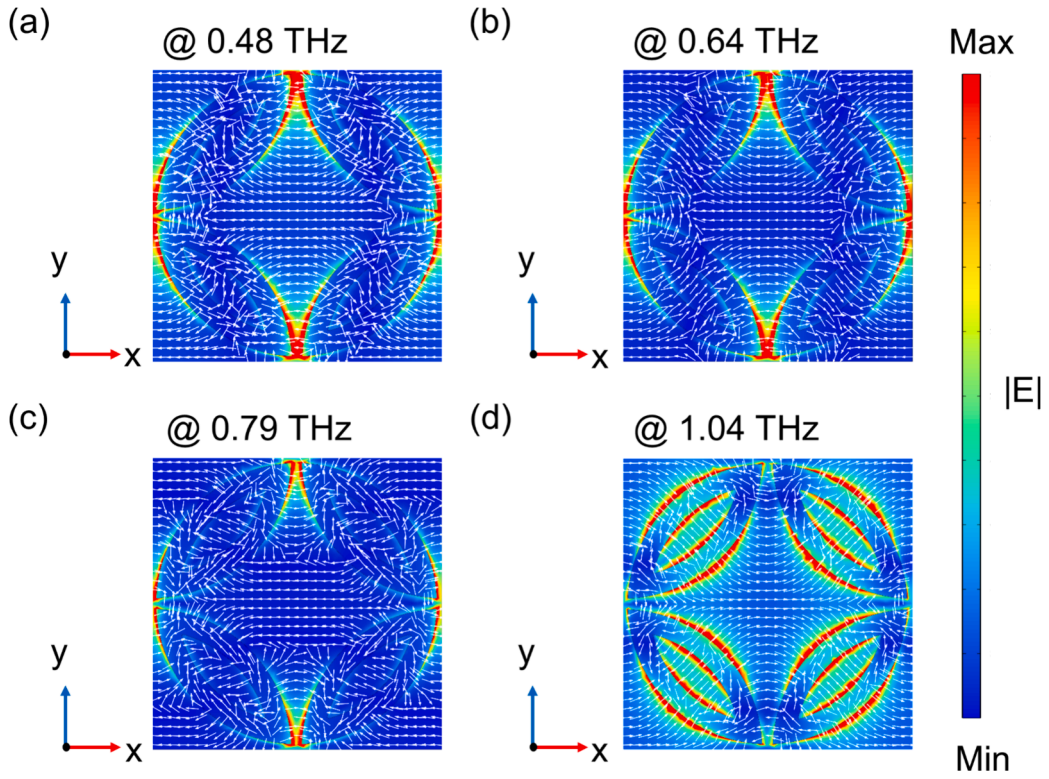

Fig. 3. Electric-field distributions at resonant frequencies in the xy plane. TE-polarized wave at (a) f = 0.48 THz, (b) f = 0.64 THz, (c) f = 0.79 THz and (d) f = 1.04 THz.

with increasing frequency, the electric field is mainly localized near the metal long-arm slit, as shown in Fig. 3d, when the absorption peaks increase due to the highly localized electric field. Fig. 4a-4d clearly show that when the incident terahertz wave is modulated by the x-component polarisation, the x-component exhibits positive and negative directions, respectively, which affects the quadrupole [36]. According to Fig. 3 and Fig. 4, it can be found that the direction of the current between the top and bottom metal layers is the same, while it is observed that at 0.48 THz, the external electric field moves in the opposite direction to the internal electric field of the metal, this is due to the fact that the internal field strength is 0 at the beginning and the metal is under the action of the external field, the internal charge is constantly moving and a charge distribution is formed on the surface of the metal which is opposite to the external electric field. In the frequency range of 0.64 THz and 0.79 THz, the direction of the electrons inside the metal is the same as the external electric field, and the electric field drives the conducting electrons to oscillate inside the particles, which results in the formation of a dipole resonance mode, where the energy collects at the four tip positions and resonance is formed between the neighboring tips. The dipole resonance mode is red-shifted to form a broad-spectrum resonance, and a multipole resonance is generated in the high-frequency region of 1.04 THz, and the energy is mainly gathered around the metal bar. Multipolar resonance is a sub-radiant resonance, and its radiative decay is weaker than that of the dipole resonance, so the peak of the spectrum is narrower. In addition, the striped arms of gold function as charge transfer, creating a head-to-tail closed current distribution between neighboring bobbins.

In many optical sensor studies, there's a heightened emphasis on achieving polarization-independent. Fig. 5a shows the transmission response for polarization angles (ϕ) from 0° to 90°, indicating that the transmittance is not affected by polarization due to the symmetry of the structure [37]. The transmission is insensitive to the polarization of incident electromagnetic waves as the quarter ring pattern structure possesses high rotational symmetry around its central axis. When incident waves interact with these highly symmetric structures, the

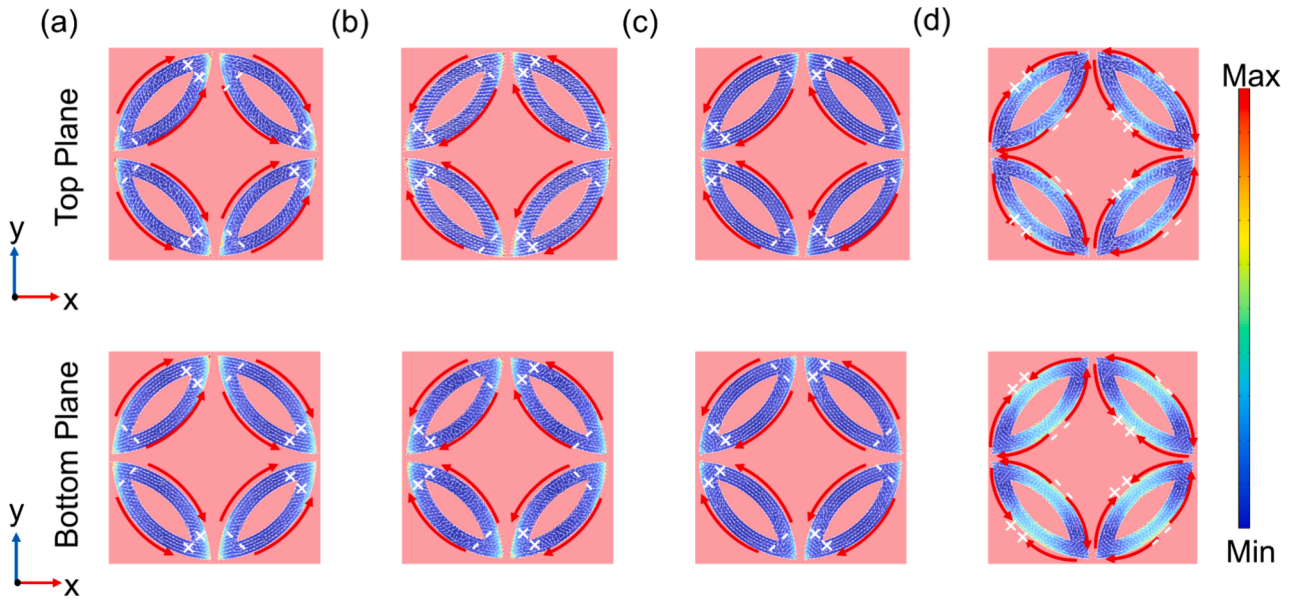

Fig. 4. Surface current distribution for top plane and bottom plane at (a) f = 0.48 THz, (b) f = 0.64 THz, (c) f = 0.79 THz and (d) f = 1.04 THz.

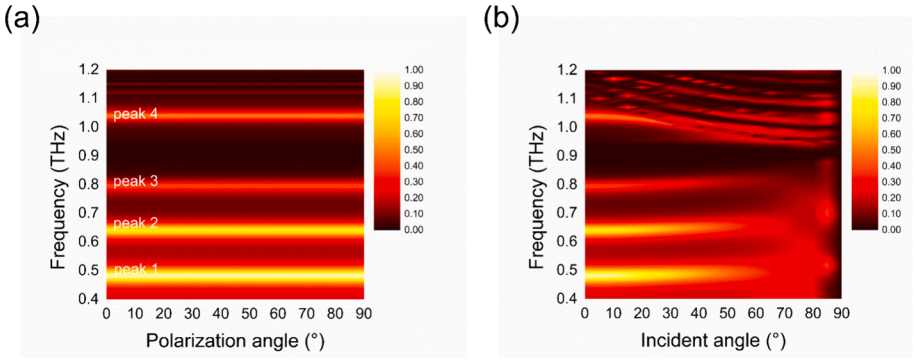

Fig. 5. Transmittance of the proposed sensor at different (a) polarization (ϕ) and (b) incident angles (θ) of the TE-polarized wave.

orientation or polarization of the incident waves doesn't significantly affect the transmission properties. The quarter ring pattern structure's insensitivity to polarization may also stem from its specific electromagnetic coupling mechanisms. In addition, the angle of incidence (θ) from 0° to 60° is shown in Fig. 5b, which indicates that the sensor is very sensitive to the angle of incidence and can accept signals at larger angles, taking advantage of the angle sensitivity.

After analyzing the peak principles, the designs of the metamaterial sensors were optimized. As shown in Fig. 6a, the variation of the quarter ring width w is investigated by determining the outer radius of the metal graph R = 53 μm. It is found that as the width of w increases, i.e., the metal quarter ring becomes wider, it leads to a blue shift of the peak 4, at the same time, the transmission peak frequency increases with the increase of w. The peak frequency of the peaks is then optimized by

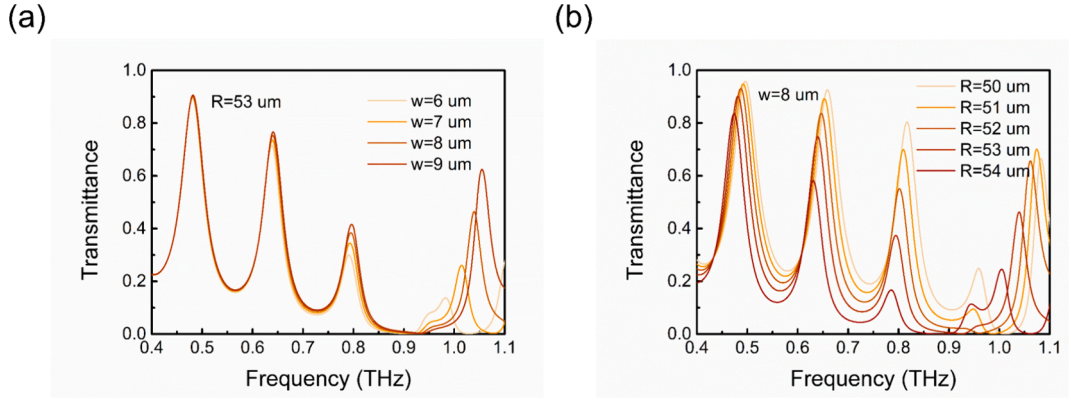

Fig. 6. (a) Simulated transmittance spectra of the proposed sensor when varying w, (b) Simulated transmittance spectra of the proposed sensor with varying R.

selecting a suitable width of the metal quarter ring w = 8 μm. Based on the variation shown in Fig. 6a, a suitable width of the metal quarter ring w = 8 μm is selected as shown in Fig. 6b and the effect of varying the size of the metal quarter ring is investigated by varying the outer radius of the metal quarter ring R. It is found that as the size of the metal quarter ring increases, the distance between the skeletonized gaps increases resulting in a red shift of the frequency resonance and a decrease in the frequency values of all the four transmission peaks. The sensitivity and linear fitting factors for each geometric parameter can be calculated by further analysis of the results. It is easy to see from the effect of changes in the geometric parameters that the resonance peak 4 has a high sensitivity characteristic. Fig. S1 clearly shows that the resonant frequency displacement is positively correlated with the increase in the width of the metal. The calculated the sensitivity value of peak 4 is 28.35 GHz/um when the geometric parameter w varies. Fig. S2 shows that the resonant frequency displacement is negatively correlated with the increase in the outer radius of the gold metal ring. The calculated value of the sensitivity of the geometric parameter R is 19.55 GHz/um at peak 4.

In addition, we investigated the effect of silicon substrate thickness on the transmittance spectra of structure, as shown in Fig. 7a, where the resonance frequencies of the first three peaks are red-shifted as the substrate thickness increases. Determining the metal size and varying the period size, it can be seen in Fig. 7b that the first two peak frequencies are blue-shifted as the period increases, and the frequency resonance peaks higher than 0.7 THz increase, which is very much due to the designed structure. It can be seen that the substrate thickness has a significant effect on the resonance frequency.

After the optimal structure selection, we investigated the sensor performances by varying the refractive index, as shown in Fig. 8b, which shows the correlation between transmission spectra amd different RI values of the tested analytes, the resonance peaks were red-shifted as the RI increased. In Fig. 8c, it is shown that varying the thickness of the analyte has little effect on the ransmittance spectra for 0.48 THz, 0.64 THz, 0.79 THz and 1.04 THz peaks. Fig. 9a-9d plot the linear fittings of the resonance frequencies to the refractive index of the analyte, and the refractive index sensitivities for the resonance frequencies were 6.84 GHz/RIU, 7.42 GHz/RIU, 8.22 GHz/RIU, and 32.11 GHz/RIU, respectively.

After we selected the optimal structure, the background refractive index was set to 1, and the temperature was changed from 0 °C to 100 °C in steps of 20 °C. We further investigated the variation of resonant frequencies with temperature. As can be seen from the data of the linear fitting in Fig. S3, the structure is so small that the coefficient of thermal expansion is negligible.

The relationship between the temperature change and the refractive index of the medium in the operating temperature range can also be expressed as [38],

$$\Delta n = \alpha \cdot n \cdot \Delta T \tag{9}$$

Here, n is the medium refractive index, α is the medium thermo-optic coefficient, and ΔT is the magnitude of the temperature change. In the terahertz band, the temperature sensitivity is modelled using the thermo-optic coefficient of silicon, which is 1.86×10^{-4}/°C [39]. It can be seen from Fig. 10 that all four peaks are red-shifted when the temperature increase. The linear fitting curve is shown in Fig. 11, their frequency shifts are all smaller than those due to RI. From this, four parameters can be obtained and RI and temperature changes can be calculated using Eq. (10),

$$\begin{bmatrix} \Delta n + \dfrac{dn}{dT} \times \Delta T \\ \Delta T \end{bmatrix} = \begin{bmatrix} 8.22\ \text{GHz/RIU} & 0.15\ \text{GHz/°C} \\ 32.11\ \text{GHz/RIU} & 0.18\ \text{GHz/°C} \end{bmatrix}^{-1} \begin{bmatrix} \Delta\lambda_1 \\ \Delta\lambda_2 \end{bmatrix} \tag{10}$$

On this basis, the effects of refractive index and temperature on the resonance peaks were investigated. The electric field distributions of the THz metamaterial at the resonance peaks are shown in Figs. 12–15, and these results indicate that the electric field is confined at the gap between the patterns. It can be seen that when the temperature increases, the effect of the resonance peak at 1.04 THz moves from the tip to the center, and the effect is insignificant at the resonance peaks at other frequencies. When the refractive index increases, the strength of the localized electric field decreases significantly.

Table 1 shows a performance comparison between the sensor proposed in this study and the sensors reported in the literature. The results show that the sensors proposed in this study are superior in terms of resonant frequency, sensitivity, Q-factor, fabrication complexity, thus they have a wide range of potential applications in sensing and detection. The quality factor (Q) is a crucial parameter in evaluating the performance of resonant sensors. A higher quality factor indicates a sharper resonance peak, which leads to better sensor performance such as sensitivity, it is because a sharper resonance peak results in larger changes in the sensor output for a given change in the measured parameter. Our data further supports the trend of correlations between the quality factor and sensor performances (6.84 GHz/RIU, 7.42 GHz/RIU, 8.22 GHz/RIU and 32.11 GHz/RIU, and quality factor Q of 6.76, 9.63, 15.51 and 26.28). For practical applications, high-quality factor THz sensors have many advantages, such as narrow resonance peaks, good stability, long service life, more sensitive response to external disturbances, faster response characteristicsand high signal-to-noise ratio.

The proposed THz metamaterial sensors can be easily fabricated using existing techniques such as photolithography, thermal evaporation and reactive etching. There are some recommendations or considerations for experimental validation of the proposed sensor: 1. The sizes of the patterned structures will be measured and their influences on the resonance peaks should be studied. 2. The terahertz time-domain

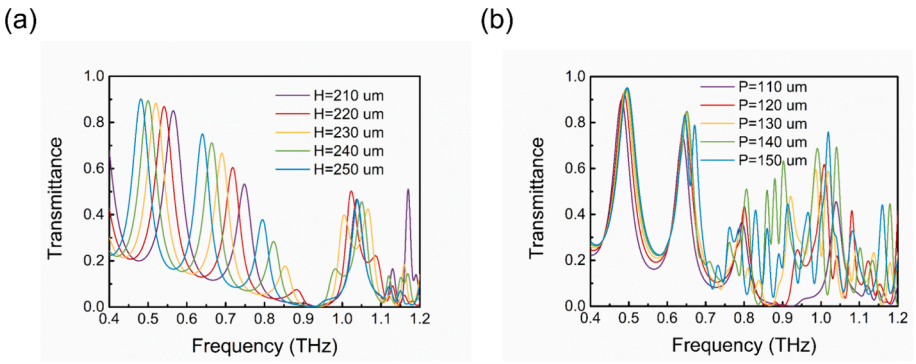

Fig. 7. Simulated transmittance spectra of the proposed THz sensor (a) when varying H, (b) when varying P.

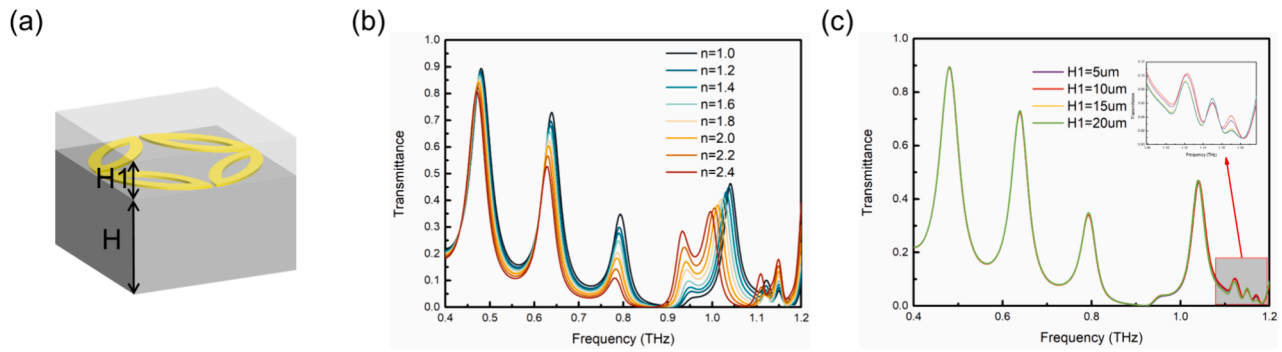

Fig. 8. (a) Schematic diagram of a nuit cell with the analyte, (b) Transmittance curves for different refractive index analytes, (c) Transmittance curves of analytes of different thickness.

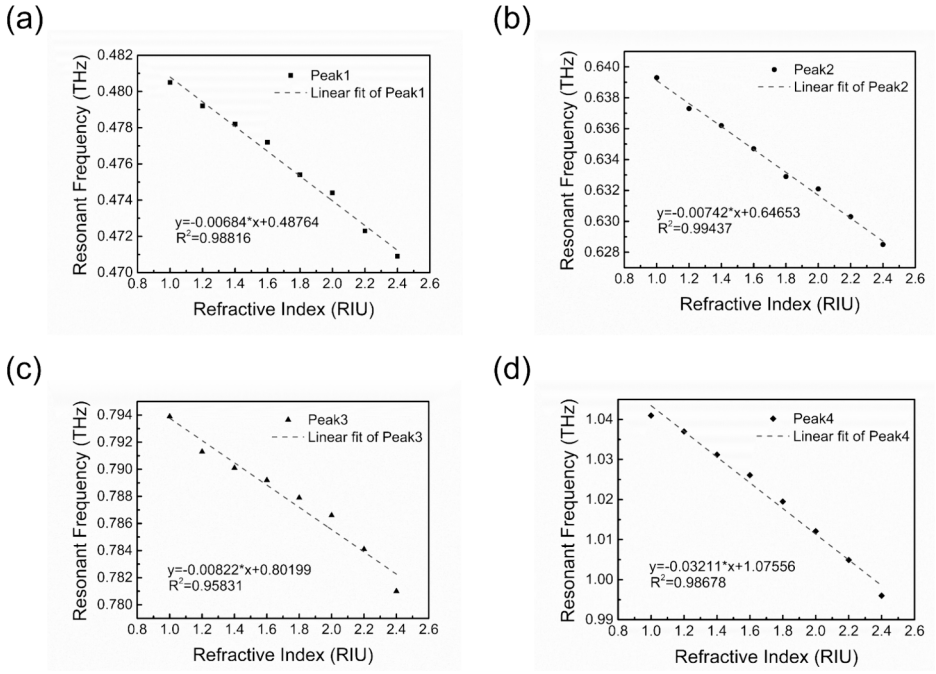

Fig. 9. The resonant frequency shift and transmittance magnitude as a function of refractive index. The frequency shifts of the resonance with increasing refractive index for the x-polarized incident THz wave. The dashed lines are linear fittings of the data.

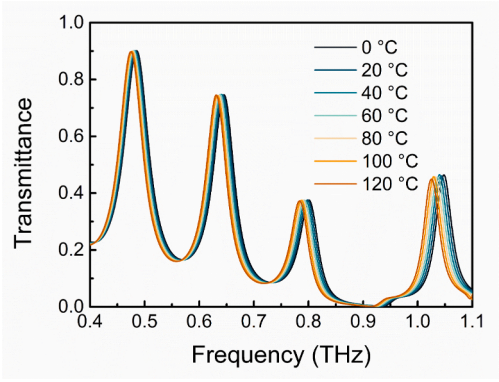

Fig. 10. The transmittance curves of R = 53 μm, w = 8 μm at different temperatures.

spectroscopy (THz-TDS) could be used to obtain the spectra of the samples. The THz-TDS test setup will need to be modified with a temperature control stage and drop on chip holder, to ensure the tests of the temperature and refractive index sensors. 3. The data will need to be extracted and compared with the simulated results, the temperature sensing performances will be compared with the data obtained by thermistors, the refractive index sensing data will be compared with the reported results. 4. Bio samples and microfluid devices will be used to explore the potential uses of the proposed sensors.

4. Conclusion

In summary, a terahertz metamaterial resonator based on a single-layer quarter ring pattern is proposed for multi-parameter terahertz sensing applications. To understand the resonance mechanisms, field finite element numerical simulations were carried out to obtain the absorption/transmittance peaks and the electromagnetic mechanisms.

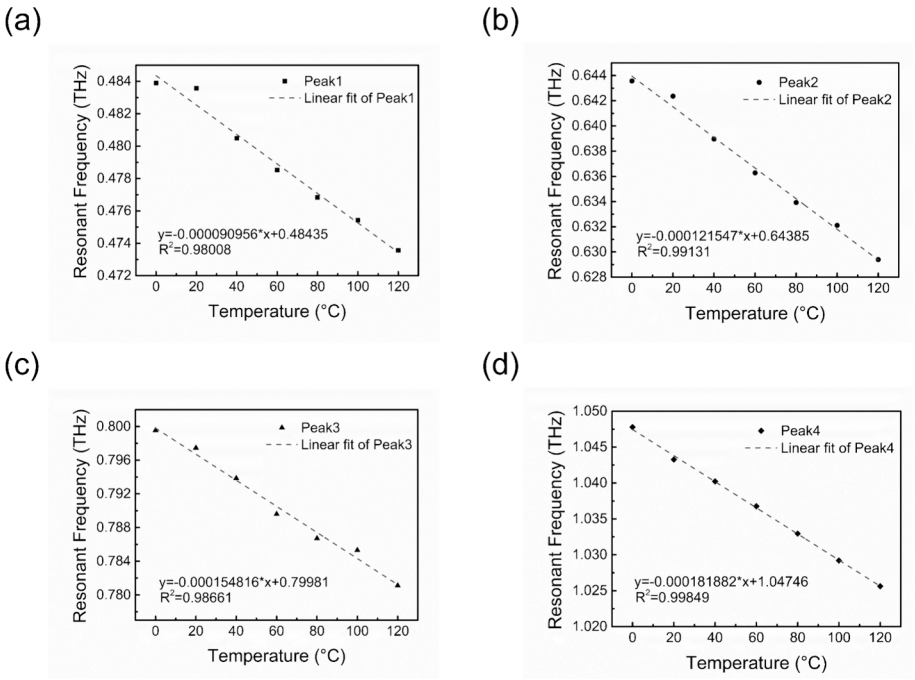

Fig. 11. The resonant frequency shift an as a function of temperature. For x-polarized incident terahertz waves, the resonant frequency are red-shifted with increasing temperature. The dashed line is a linear fitting of the data. (For interpretation of the references to colour in this figure legend, the reader is referred to the web version of this article.)

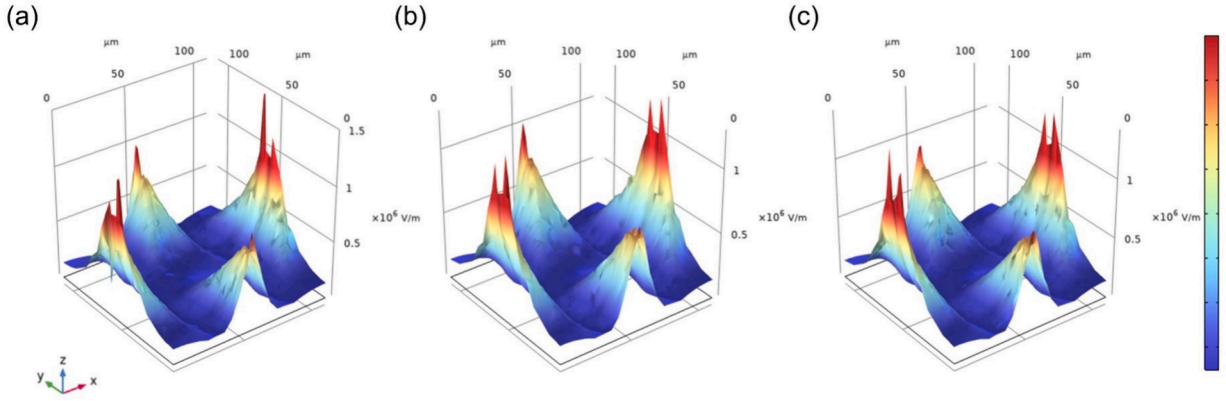

Fig. 12. The electric field distributions at 0.48 THz when (a) n = 1.2, T = 20 °C, (b) n = 1.2, T = 60 °C, and (c) n = 1.4, T = 60 °C.

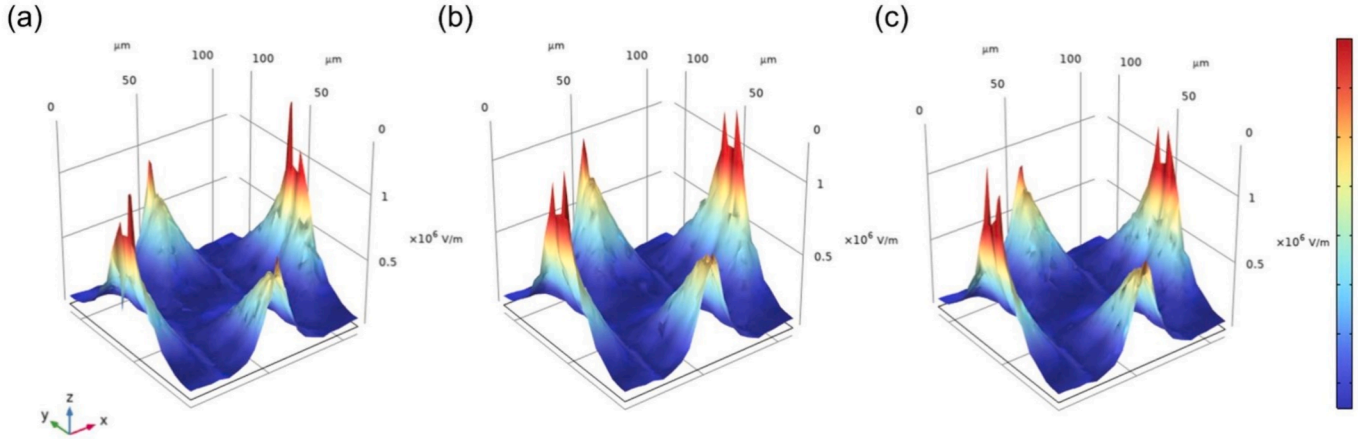

Fig. 13. The electric field distributions at 0.64 THz when (a) n = 1.2, T = 20 °C, (b) n = 1.2, T = 60 °C, and (c) n = 1.4, T = 60 °C.

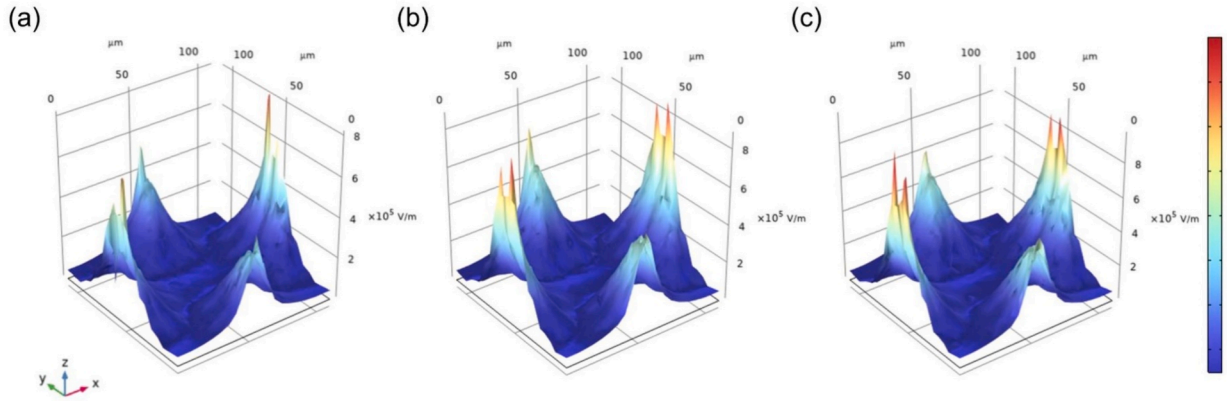

Fig. 14. The electric field distributions at 0.79 THz when (a) n = 1.2, T = 20 °C, (b) n = 1.2, T = 60 °C, and (c) n = 1.4, T = 60 °C.

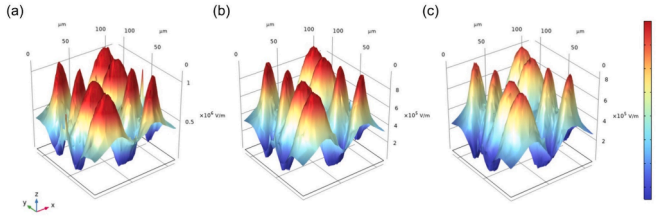

Fig. 15. The electric field distributions at 1.04 THz when (a) n = 1.2, T = 20 °C, (b) n = 1.2, T = 60 °C, and (c) n = 1.4, T = 60 °C.

Table 1
Performance comparison with other relevant THz sensors.

Description	Resonant frequency (THz)	Sensitivity (GHz/RIU)	Q-factor	Fabrication complexity	Multi-parameter
Cross-patterned metal layer with silicon layer [40]	0.6	7.0	11.6	Medium	no
Metal strips with double split gap squares [41]	0.402	27.3	9.6	Low	no
I-shaped metal strip [42]	0.6	18.0	6.0	Low	no
Grating array structure with silicon layer [43]	1.66	–	23.45	High	no
Square ring with T-shaped strips [44]	1.103	37.0		Low	no
Single-Layer Quarter Ring Patterns with silicon substrate [This work]	1.04	32.11	26.28	Low	yes

The resonant frequencies of transmission are 0.48 THz, 0.64 THz, 0.79 THz, and 1.04 THz, the transmittances are 93.7 %, 79.1 %, 38.4 %, and 50.8 %, respectively. The refractive index sensitivity of resonant frequencies is 6.84 GHz/RIU, 7.42 GHz/RIU, 8.22 GHz/RIU, and 32.11 GHz /RIU, with a quality factor Q of 6.76, 9.63, 15.51 and 26.28, respectively. The temperature sensitivities at resonant frequencies are 0.09 GHz/°C, 0.12 GHz/°C, 0.15 GHz/°C, and 0.18 GHz/°C, respectively. The designed terahertz metamaterial resonators can be used as refractive index, temperature and bio sensors. This method has the advantages of simple structure, easy processing, easy miniaturization and high sensitivity, and has a wide range of potential applications in chemical and biological sensing. The research results of this paper will also provide higher reliability and accuracy for many fields, such as industry process control, microfluid devices, wireless communication, environmental monitoring and so on.

CRediT authorship contribution statement

Sijia Du: Writing – original draft, Visualization, Validation, Investigation, Formal analysis, Data curation. **Xiaoman Li:** Writing – original draft, Visualization, Validation, Investigation, Formal analysis, Data curation. **Mohsin Raza:** Data curation, Formal analysis, Investigation, Validation, Visualization, Writing – review & editing. **Chenlu Mao:** Visualization, Validation, Formal analysis. **Fulong Yao:** Visualization, Validation, Formal analysis. **Yinghao Yuan:** Writing – review & editing, Supervision, Project administration. **Weiping Wu:** Writing – review & editing, Writing – original draft, Supervision, Project administration, Funding acquisition, Conceptualization.

Declaration of competing interest

The authors declare that they have no known competing financial interests or personal relationships that could have appeared to influence the work reported in this paper.

Data availability

Data will be made available on request.

Acknowledgments

This work is supported by the National Key R&D Program of China (No. 2021YFB2800703, 2021YFB2800701, 2021YFB2800700), the National Natural Science Foundation of China (NSFC No. 52273242), the China Science and Technology Cloud (CSTCloud), the Alliance of International Science Organizations (ANSO) (http://www.anso.org.cn accessed on) for awarding The ANSO Scholarship for Young Talents and the Chinese Academy of Sciences.

Appendix A. Supplementary data

Supplementary data to this article can be found online at https://doi.org/10.1016/j.optlastec.2024.111085.

References

[1] T. Nagatsuma, G. Ducournau, C.C. Renaud, Advances in terahertz communications accelerated by photonics, Nat. Photonics 10 (6) (2016) 371–379.

[2] J.M. Jornet, E.W. Knightly, D.M. Mittleman, Wireless communications sensing and security above 100 GHz, Nat. Commun. 14 (1) (2023) 841.
[3] C.M. Watts, D. Shrekenhamer, J. Montoya, G. Lipworth, J. Hunt, T. Sleasman, S. Krishna, D.R. Smith, W.J. Padilla, Terahertz compressive imaging with metamaterial spatial light modulators, Nat. Photonics 8 (8) (2014) 605–609.
[4] W.W. Tang, A. Politano, C. Guo, W.L. Guo, C.L. Liu, L. Wang, X.S. Chen, W. Lu, Ultrasensitive room-temperature terahertz direct detection based on a bismuth selenide topological insulator, Adv. Funct. Mater. 28 (31) (2018) 1801786.
[5] H.T. Chen, W.J. Padilla, J.M.O. Zide, A.C. Gossard, A.J. Taylor, R.D. Averitt, Active terahertz metamaterial devices, Nature 444 (7119) (2006) 597–600.
[6] Y.L. Chen, B.B. Wang, Y.Z. Zang, C.S. Zhang, H.X. Zhang, Y. Yuan, D.L. Zhou, L. W. Hou, M. Pan, X.D. Wang, The high-performance imaging verification of Si: P blocked impurity band detector for very-long-wave-infrared spectral range, IEEE J. Quantum Electron. 56 (3) (2020) 4000506.
[7] Q. Qiu, Z. Huang, Photodetectors of 2D materials from ultraviolet to terahertz waves, Adv. Mater. 33 (15) (2021) e2008126.
[8] X.Q. Zhang, Q. Xu, L.B. Xia, Y.F. Li, J.Q. Gu, Z. Tian, C.M. Ouyang, J.G. Han, W. L. Zhang, Terahertz surface plasmonic waves: a review, Adv. Photonics 2 (1) (2020) 014001.
[9] T.L. Cocker, V. Jelic, R. Hillenbrand, F.A. Hegmann, Nanoscale terahertz scanning probe microscopy, Nat. Photonics 15 (8) (2021) 558–569.
[10] N.I. Landy, S. Sajuyigbe, J.J. Mock, D.R. Smith, W.J. Padilla, Perfect metamaterial absorber, Phys. Rev. Lett. 100 (20) (2008) 207402.
[11] K.V. Sreekanth, Y. Alapan, M. ElKabbash, E. Ilker, M. Hinczewski, U.A. Gurkan, A. DeLuca, G. Strangi, Extreme sensitivity biosensing platform based on hyperbolic metamaterials, Nat. Mater. 15 (6) (2016) 621–627.
[12] M. Vidal, M.S. Soares, M. Loyez, F.M. Costa, C. Caucheteur, C. Marques, S. O. Pereira, C. Leitao, Relevance of the spectral analysis method of tilted fiber bragg grating-based biosensors: a case-study for heart failure monitoring, Sensors 22 (2022) 2141.
[13] X. Li, X. Xu, H. Zhou, Y. Gu, F. Liu, W. Wu, Ultra-broadband tunable terahertz absorber of graphene and hierarchical plasmonic metamaterials, Adv. Dev. Instrum. 4 (2023) 0014.
[14] K.L. Chen, C.J. Ruan, Y.H. Cao, SRRs and cross combine asymmetric metamaterials promising for THz sensor, IEEE ICMMT 2020 (2020) 1–3.
[15] H. Tao, A.C. Strikwerda, Performance enhancement of terahertz metamaterials on ultrathin substrates for sensing applications, Appl. Phys. Lett. 97 (26) (2010) 261909.
[16] X.M. Li, H. Feng, M.J. Yun, Z. Wang, Y.G. Hu, Y.J. Gu, F.H. Liu, W.P. Wu, Polarization-independent and all-optically modulated multiband metamaterial coherent perfect absorber, Opt. Laser Technol. 166 (2023) 109644.
[17] K. Xu, Integrated silicon directly modulated light source using p-well in standard CMOS technology, IEEE Sens. J. 16 (2016) 6184–6191.
[18] J.B. Pendry, Negative refraction makes a perfect lens, Phys. Rev. Lett. 85 (18) (2000) 3966–3969.
[19] T. Low, A. Chaves, J.D. Caldwell, A. Kumar, N.X. Fang, P. Avouris, T.F. Heinz, F. Guinea, L. Martin-Moreno, F. Koppens, Polaritons in layered two-dimensional materials, Nat. Mater. 16 (2) (2017) 182–194.
[20] A.S. Saadeldin, M.F.O. Hameed, E.M.A. Elkaramany, S.S.A. Obayya, Highly sensitive terahertz metamaterial sensor, IEEE Sens. J. 19 (18) (2019) 7993–7999.
[21] M.R. Nickpay, M. Danaie, A. Shahzadi, Highly sensitive THz refractive index sensor based on folded split-ring metamaterial graphene resonators, Plasmonics 17 (1) (2021) 237–248.
[22] T.J. Kippenberg, A.L. Gaeta, M. Lipson, M.L. Gorodetsky, Dissipative Kerr solitons in optical microresonators, Science 361 (6402) (2018) eaan8083.
[23] L. Zhao, J.Y. Wang, H.Y. Li, Simultaneous sensing of refractive index and temperature using a symmetry-breaking silicon metasurface with multiple Fano peaks, in: 2021 IEEE 16th International Conference on Nano/Micro Engineered and Molecular Systems (NEMS), 2021, pp. 1441–1446.
[24] R. Singh, W. Zhang, X. Liu, B. Zhang, S. Kumar, WaveFlex biosensor: MXene-immobilized W-shaped fiber-based LSPR sensor for highly selective tyramine detection, Opt. Laser Technol. 171 (2024) 110357.
[25] G. Lopes, N. Cennamo, L. Zeni, R. Singh, S. Kumar, A.J.S. Fernandes, F. Costa, S. O. Pereira, C. Marques, Innovative optical pH sensors for the aquaculture sector: comprehensive characterization of a cost-effective solution, Opt. Laser Technol. 171 (2024) 110355.
[26] M.S. Soares, L.C.B. Silva, M. Vidal, M. Loyez, M. Facao, C. Caucheteur, M.E. V. Segatto, F.M. Costa, C. Leitao, S.O. Pereira, N.F. Santos, C.A.F. Marques, Label-free plasmonic immunosensor for cortisol detection in a D-shaped optical fiber, Biomed. Opt. Express 13 (6) (2022) 3259–3274.
[27] X. Liu, R. Singh, M. Li, G. Li, R. Min, C. Marques, B. Zhang, S. Kumar, Plasmonic sensor based on offset-splicing and waist-expanded taper using multicore fiber for detection of Aflatoxins B1 in critical sectors, Opt. Express 31 (2023) 4783–4802.
[28] R. Singh, Z. Wang, C. Marques, R. Min, B. Zhang, S. Kumar, Alanine aminotransferase detection using TIT assisted four tapered fiber structure-based LSPR sensor: From healthcare to marine life, Biosens. Bioelectron. 236 (2023) 115424.
[29] N. Mohammad-Reza, D. Mohammad, S. Ali, Design of a graphene-based multi-band metamaterial perfect absorber in THz frequency region for refractive index sensing, Phys. E 138 (2022) 115114.
[30] H. Liu, F. Pang, H. Guo, W. Cao, Y. Liu, N. Chen, Z. Chen, T. Wang, In-series double cladding fibers for simultaneous refractive index and temperature measurement, Opt. Express 18 (2010) 13072–13082.
[31] Y. Zhang, Y.K. Liu, J.G. Han, Electrically tunable resonant terahertz transmission in subwavelength hole arrays, Chin. Phys. B 23 (2014) 067301.
[32] K. Xu, Silicon electro-optic micro-modulator fabricated in standard CMOS technology as components for all silicon monolithic integrated optoelectronic systems, J. Micromech. Microeng. 31 (2021) 054001.
[33] B. Dong, C. Zhang, G. Guo, X. Zhang, Y. Wang, L. Huang, H. Ma, Q. Cheng, BST-silicon hybrid terahertz meta-modulator for dual-stimuli-triggered opposite transmission amplitude control, Nanophotonics 11 (2022) 2075–2083.
[34] M. Zhang, Z. Ma, Polarization-independent multi-resonance with high q-factor for highly sensitive terahertz sensors based on all-dielectric metasurface, IEEE Photonics J. 14 (4) (2022) 1–8.
[35] N. Mohammad-Reza, D. Mohammad, S. Ali, Graphene-based metamaterial absorber for refractive index sensing applications in terahertz band, Diamond Relat. Mater. 130 (2022) 109539.
[36] S.T. Huang, S.F. Hsu, K.Y. Tang, T.J. Yen, D.J. Yao, Application of a terahertz system combined with an X-shaped metamaterial microfluidic cartridge, Micromachines 11 (2020) 74.
[37] M.L. Hakim, T. Alam, M.S. Soliman, N.M. Sahar, M.H. Baharuddin, S.H.A. Almalki, M.T. Islam, Polarization insensitive symmetrical structured double negative (DNG) metamaterial absorber for Ku-band sensing applications, Sci. Rep. 12 (2022) 479.
[38] Z.X. Chen, B.M. Liang, S.L. Zhuang, Study on photonic crystal-based temperature sensor at terahertz band, Opt. Instrum. 41 (2019) 56–59.
[39] M.V. Exter, D. Grischkowsk, Carrier dynamics of electrons and holes in moderately doped silicon, Phys. Rev. B 41 (17) (1990) 12140–12149.
[40] L. Cong, S. Tan, R. Yahiaoui, F. Yan, W. Zhang, R. Singh, Experimental demonstration of ultrasensitive sensing with terahertz metamaterial absorbers: a comparison with the metasurfaces, Appl. Phys. Lett. 106 (2015) 031107.
[41] M. Gupta, Y.K. Srivastava, M. Manjappa, R. Singh, Sensing with toroidal metamaterial, Appl. Phys. Lett. 110 (2017) 121108.
[42] M. Gupta, R. Singh, Terahertz sensing with optimized Q/V_{eff} metasurface cavities, Adv. Opt. Mater. 8 (16) (2020) 1902025.
[43] X. Zhang, Y. Wang, Z. Cui, L. Yue, X. Zhang, C. Yang, X. Wang, A novel THz metasurface sensor based on the integration of carbon nanotube film and grating silicon microfluidic channel, in: 46th International Conference on Infrared, Millimeter and Terahertz Waves (IRMMW-THz), 2021, pp. 1–2.
[44] D. Wang, K.D. Xu, S. Luo, Y. Cui, L. Zhang, J. Cui, A high Q-factor dual-band terahertz metamaterial absorber and its sensing characteristics, Nanoscale 15 (2023) 3398–3407.